

# FOREIGN OBJECT SEGMENTATION IN CHEST X-RAYS THROUGH ANATOMY-GUIDED SHAPE INSERTION

Constantin Seibold<sup>1</sup>, Hamza Kalisch<sup>1</sup>, Lukas Heine<sup>1</sup>, Simon Reiß<sup>2</sup>, Jens Kleesiek<sup>1</sup>

<sup>1</sup>University Medicine Essen <sup>2</sup>Karlsruhe Institute of Technology

## ABSTRACT

In this paper, we tackle the challenge of instance segmentation for foreign objects in chest radiographs, commonly seen in postoperative follow-ups with stents, pacemakers, or ingested objects in children. The diversity of foreign objects complicates dense annotation, as shown in insufficient existing datasets. To address this, we propose the simple generation of synthetic data through (1) insertion of arbitrary shapes (lines, polygons, ellipses) with varying contrasts and opacities, and (2) cut-paste augmentations from a small set of semi-automatically extracted labels. These insertions are guided by anatomy labels to ensure realistic placements, such as stents appearing only in relevant vessels. Our approach enables networks to segment complex structures with minimal manually labeled data. Notably, it achieves performance comparable to fully supervised models while using 93% fewer manual annotations.

## 1. INTRODUCTION

Chest radiographs (CXR) are essential for detecting thoracic FBs, monitoring post-surgical complications, confirming proper placement of devices (e.g., stents, catheters), and identifying retained surgical instruments. The variety of foreign bodies (FB) types complicates dataset creation for detection and segmentation, requiring annotators to identify categories and manage overlapping objects [1]. While current datasets often focus on specific FB subcategories [2, 3], this work simplifies automatic FB detection and segmentation in CXR to (1) improve anomaly statistics and (2) facilitate dataset generation by categorizing pre-extracted masks. We hypothesize that most FBs are distinguishable by their high contrast and opacity in X-rays, often appearing prominently. Using domain knowledge of geometric structures – such as circles (e.g., coins), rings (e.g., heart valves), grids (e.g., stents), and lines (e.g., pacemaker wires) – we synthetically generate data with precise ground truth, which enable the training of most recent instance segmentation methods. By incorporating anatomy segmentation [1, 4], we model FBs like stents at vascular sites such as the aorta. These structures are inserted into patient models using OpenCV or Matplotlib. We also employ a cut-paste approach [5, 6] to insert real-world structures (e.g., pacemakers, port catheter tips) with varying

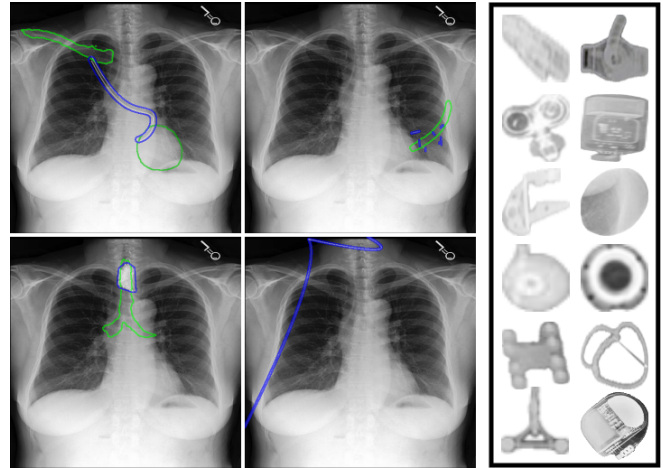


**Fig. 1.** **Left:** We display some plotted structures using anatomical guidance. From top left to bottom right as follows: Parallel lines from the clavicle to a ventricle, surgical clips at a rib, a grid structure at the trachea, a general line. **Right:** We display a subset for the different more composite foreign objects.

contrast, covering a wide range of FBs with fewer than 140 instance annotations.

Our goal here is *not* to generate realistic images to the human eye, but rather create images which enable a neural network to identify FB and general non-organic elements in real data without significant manual annotation effort.

We benchmark our data generation pipeline using four state-of-the-art instance segmentation models, assessing their transfer to real data. Mask2Former [7] achieves the best performance, rivaling models which were trained on a dataset with an additional 93% annotations. Further, when considering other instance segmentation methods it can be observed that the inclusion of synthetic material substantially improves performance. We will make our code publicly available.

Our key contributions summarize as follows:

1. We develop and release a cost-efficient data generation pipeline for instance segmentation research.
2. We introduce the first FB instance segmentation approach in CXR based on synthetic data, using class-agnostic methods to recognize a broad range of FBs.

## 2. ANATOMY-GUIDED STRUCTURE INSERTION

Our data generation pipeline is outlined in Figure 2. We begin by defining a set of images without foreign bodies (FBs),  $src\_imgs$ , which we determine by filtering the MIMIC-CXR dataset [8] via their image-level labels. For each image in  $src\_imgs$ , we apply an anatomy segmentation model  $anat(img)$ , trained on the PAXRay++ dataset [1, 4], with which we extract up to 158 anatomies.

In the synthetic dataset generation process, we begin by randomly determining the number of annotations,  $num\_ann$ , for each sample, where this value is selected between 1 and a predefined maximum,  $max\_annotations$ . Next, we randomly sample a subset of anatomical regions,  $A \subset anat(cur\_img)$ , from the current image,  $cur\_img$ .

For each annotation on  $cur\_img \in src\_imgs$ , we randomly assign an annotation type,  $ann\_type \in$  Structure Plotting, Cut-Paste determining the operation applied to the image. If  $ann\_type$  is ‘Structure Plotting’, we insert a structure at the positions of the sampled anatomical regions. If it is ‘Cut-Paste’, we cut and paste a portion of the image in the region.

This process is repeated until the number of annotations,  $num\_ann$ , for the image is reached. Next, we describe the two annotation types.

### 2.1. Structure Plotting

We generate nine different types of structures by randomly sampling their position, greyscale value, size, and opacity:

- **Textual Structures:** These represent text seen in CXRs, such as scan orientation markers or accessory labels. We sample a random ASCII string, font size, and type, with the text either dark, bright, or with transparent background. The text is not anchored to specific anatomy.
- **Circular Structures:** Objects like prosthetics, coins, or ECG sensors resemble dense, whitish circular structures. We sample an ellipse with random width, height, and rotation, inserting it into organs or the humerus.
- **Ring-like Structures:** Rings, such as cerclage wires or artificial valves, are modeled as ellipses with varying line thickness. These hollow structures are inserted into anatomical regions.
- **Rectangular Structures:** Medical devices like event recorders or catheter ports often have rectangular shapes. We sample a random bounding box, filled with varying greyscale and opacity, without anatomical anchoring.
- **Clip-like Structures:** Surgical clips, which may be left inside the body after procedures, are represented by small lines of varying thickness around anatomical structures.
- **Grid-like Structures:** Stents are modeled by a randomized grid spanning an anatomical mask, where each node has up to four neighbors. The grid is randomly shaded.
- **Lines:** Catheters, sensors, or accessories such as necklaces appear as line-like structures. We generate up to five

connected Bezier curves, starting outside the body with random thickness.

- **Parallel Lines:** Tubular structures like endotracheal tubes are modeled by two parallel Bezier curves, enclosing a random greyscale space with random thickness.

### 2.2. Cut-Paste of Pre-extracted FB Crops

For complex structures unsuitable for directly plotting them onto the image, we collect a small set of cutout instances ( $cut\_outs$ ). Cutout examples for each of the different object categories are displayed in Fig. 1.

The Cut-Paste process is then carried out as follows: Given a sampled anatomical structure  $A$ , we randomly sample a crop, apply weak augmentations, and insert it into the area of a random anatomical structure using either seamless or normal Poisson editing [9], or non-smoothed insertion [6].

## 3. EXPERIMENTAL SETUP

### 3.1. Implementation Details

We perform dataset generation utilizing both Matplotlib and OpenCV. Our model implementation is based on the MMDetection library and the models were trained on an A40 GPU with a multiscale input resolution ranging from (384, 384) to (896, 896). Our evaluation metric is Mask Mean Average Precision (mAP) and Mask Mean Average Recall (mAR). During training, we applied data augmentation techniques such as RandomResizedCrop, RandomFlip, and RandAugment [10]. The batch size was set to 16 with the rest of the hyperparameters adhering to the definitions in the respective method [11]. The models (QueryInst [12], PointRend [13], SparseInst [14], Mask2Former [7]) were trained for 30K iterations. For testing, we employ no test time augmentation.

### 3.2. Datasets

**SynthFB:** Using our proposed pipeline we generate a synthetic dataset in a stepwise fashion to facilitate robust training of image recognition models. The source data originates from a curated subset of MIMIC-CXR [8], comprising 4,769 images selected to exclude any foreign bodies. For the manual created cutouts, we create 140 manual instance mask annotations and store the masked-out region. We set  $max\_annotations = 12$ . The dataset encompasses multiple subsets, ranging from 500 to a maximum of 30,000 synthetic images. Additionally, a distinct validation set with 2,500 images is generated independently to assess performance.

**MFidB:** For some examples from Kildal *et al.* [15], there exist detailed colored annotations for foreign medical objects. Through simple color filtering and alignment, one can extract pixel-wise masks for further instance segmentation purposes. After extracting the annotations through the images with and

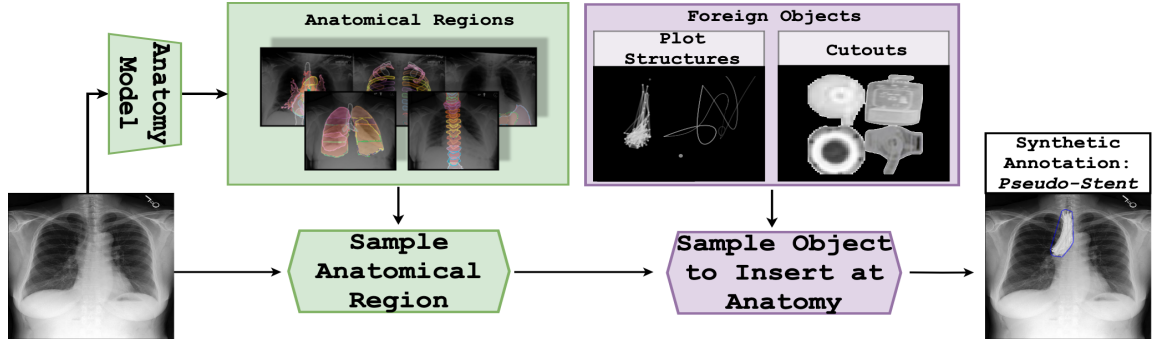


**Fig. 2.** Pseudo Foreign Object insertion via Anatomical Guidance. After segmenting anatomical structures of a given CXR, we sample either a cutout or a synthetic structure to be plotted. Using the sample, we then simulate a foreign body at the corresponding anatomical position by either inserting or plotting the structure.

without coloring, the FB can be obtained. We gained access to this dataset by Albrecht [16] upon request. It consists of 400 images with 1,777 annotations for training and 104 images with 497 annotations for validation via the described approach. We term this dataset MFidB (Medizinische Fremdkörper in der Bildgebung).

## 4. EVALUATION

### 4.1. Performance on Synthetic Data

In Fig. 3, we display the effect of the number of artificially generated samples when evaluated on SynthFB. When just using 500 samples most models achieve around 30% mAP. We see that with the increase of training data the mAP rises consistently across all models. We also see that Mask2Former noticeably outperforms other methods for both small and large amounts of data as achieves close to 55% mAP at 30K samples. SparseInst, in comparison, tends to struggle more with this task, as it struggles to significantly improve until it is trained on 15K different samples.

Overall, it appears that all models are able to learn the task of foreign body instance segmentation on the data and the trend, that more data improves the performance when evaluated on the synthetic dataset holds true.

### 4.2. Transfer of Models

Next, we are interested in how models that are trained in this manner can be used to transfer to segment real data. We display the performance of models directly trained on MFidB (In-Domain) as well as the models trained on SynthFB and then evaluated on MFidB (Out-of-Domain) in Tab. 1.

We can see that Mask2Former trained on SynthFB utilizing less than 140 annotated instances manages to match the performance when trained directly on MFidB albeit using

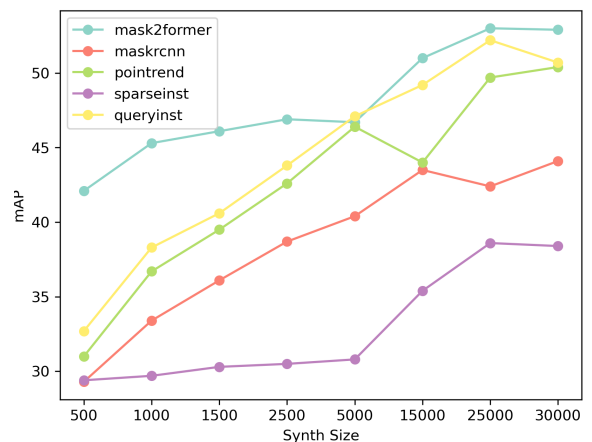


**Fig. 3.** We show the mAP performances of the five considered baselines across different artificial dataset sizes on the synthetic validation set of SynthFB.

93% less manual annotations. All models display similar if not better performance compared to their in-domain counterparts across all dataset sizes. These differences become especially apparent for SparseInst and QueryInst with more than 9 absolute points in mAP and mAR.

We, furthermore, qualitatively tested the Mask2Former model trained on SynthFB on images in the wild in Fig. 4. Here, we can see that synthetic data can assist the identification of foreign bodies also in other X-ray domains.

## 5. DISCUSSION AND CONCLUSION

In this work, we have proposed a pipeline for artificial data generation for foreign body instance segmentation that utilizes only a handful of annotated labels. We integrate expert knowledge by plotting structures that models either generalize from or can directly find as a target. We noticed that our synthetically generated data was able to provide a suitable basis



**Fig. 4.** We can see that Mask2Former trained on SynthFB is able to also segment elements in other X-ray domains[17].

for models to identify real FB in X-ray imaging. We have to note that while these results provide a pointer towards the actual performance of these models, making definite statements in that direction is difficult due to the lack of real human-curated datasets for this task. We expect that our work will foster progress in the field of foreign object segmentation and be a helpful tool in semi-automatic generation pipelines for large scale dataset annotation efforts.

## 6. COMPLIANCE WITH ETHICAL STANDARDS

This research study was conducted retrospectively using human subject data made available in open access by [8]. Ethical approval was not required as confirmed by the license attached with the open access data.

## 7. REFERENCES

- [1] Constantin Seibold et al., “Detailed annotations of chest x-rays via ct projection for report understanding,” *arXiv preprint arXiv:2210.03416*, 2022.
- [2] Jennifer SN Tang et al., “Clip, catheter and line position dataset,” *Scientific Data*, vol. 8, no. 1, pp. 285, 2021.
- [3] JF Healthcare, “Object-cxr - automatic detection of foreign objects on chest x-rays,” .
- [4] Constantin Seibold et al., “Accurate fine-grained segmentation of human anatomy in radiographs via volumetric pseudo-labeling,” *arXiv preprint arXiv:2306.03934*, 2023.

Method	In-Domain 1, 777 manual Masks		Out-of-Domain 140 manual Masks	
	mAP	mAR	mAP	mAR
PointRend	15.02	28.85	19.28 (+4.26)	27.08 (-1.77)
SparseInst	10.43	13.83	19.67 (+9.24)	23.36 (+9.53)
QueryInst	7.70	11.19	20.45 (+12.75)	24.45 (+13.26)
Mask2Former	23.54	29.56	22.94 (-0.60)	31.45 (+1.89)

**Table 1.** Performance on MFidB for models trained on it (in-domain) and trained on SynthFB (out-of-domain). We can see that most methods show similar compared to their in-domain counterparts utilizing more manual annotations.

- [5] Debidatta Dwibedi et al., “Cut, paste and learn: Surprisingly easy synthesis for instance detection,” in *Proceedings of the IEEE international conference on computer vision*, 2017, pp. 1301–1310.
- [6] Golnaz Ghiasi et al., “Simple copy-paste is a strong data augmentation method for instance segmentation,” in *Proceedings of the IEEE/CVF conference on computer vision and pattern recognition*, 2021, pp. 2918–2928.
- [7] Bowen Cheng et al., “Masked-attention mask transformer for universal image segmentation,” in *Proceedings of the IEEE/CVF conference on computer vision and pattern recognition*, 2022, pp. 1290–1299.
- [8] Alistair EW Johnson et al., “Mimic-cxr, a de-identified publicly available database of chest radiographs with free-text reports,” *Scientific data*, vol. 6, no. 1, pp. 317, 2019.
- [9] Patrick Pérez et al., “Poisson image editing,” in *Seminal Graphics Papers: Pushing the Boundaries, Volume 2*, pp. 577–582. 2023.
- [10] Ekin D Cubuk et al., “Randaugment: Practical automated data augmentation with a reduced search space,” in *Proceedings of the IEEE/CVF conference on computer vision and pattern recognition workshops*, 2020, pp. 702–703.
- [11] Kai Chen et al., “MMDetection: Open mmlab detection toolbox and benchmark,” *arXiv preprint arXiv:1906.07155*, 2019.
- [12] Yuxin Fang et al., “Instances as queries,” in *Proceedings of the IEEE/CVF international conference on computer vision*, 2021, pp. 6910–6919.
- [13] Alexander Kirillov et al., “Pointrend: Image segmentation as rendering,” in *Proceedings of the IEEE/CVF conference on computer vision and pattern recognition*, 2020, pp. 9799–9808.
- [14] Tianheng Cheng et al., “Sparse instance activation for real-time instance segmentation,” in *Proceedings of the IEEE/CVF Conference on Computer Vision and Pattern Recognition*, 2022, pp. 4433–4442.
- [15] Daniela Kildal, *Medizinische Fremdkörper in der Bildgebung: Thorax, Abdomen, Gefäße und Kinder*, Springer-Verlag, 2016.
- [16] Philipp Albrecht, “Collective confidence maps for foreign object detection in x-ray images with limited data,” .
- [17] “Ncbi bookshelf,” <https://www.ncbi.nlm.nih.gov/books/NBK470294/figure/article-21912.image.f1/>, 2024, Accessed: 2024-07-18.